PAPER

Structural and electrochemical studies of Sm@D_{3h}-C$_{74}$ reveal a weak metal–cage interaction and a small band gap species†

Wei Xu,[b] Yajuan Hao,[a] Filip Uhlik,[d] Zujin Shi,*[b] Zdenêk Slanina*[c] and Lai Feng*[a]

A metallofullerene Sm@D_{3h}-C$_{74}$ that contains a divalent rare-earth metal has been studied structurally and electrochemically. The crystallographic analysis revealed that the endohedral Sm atom is more or less motional rather than being localized at a site where the pyracylene motif is nearby. This suggests a weaker metal–pyracylene interaction in Sm@D_{3h}-C$_{74}$ relative to that in M^{II}@C$_{74}$ (M = Group II metal), thus confirming the importance of the metal variety. The electrochemical studies showed a major difference between the redox properties of Sm@D_{3h}-C$_{74}$ and other Sm-fullerenes and indicated a small band gap for the title compound.

Introduction

Since the discovery of endohedral metallofullerenes (EMFs), these species have been of great interest to researchers from various disciplines due to their unique structures as well as their unprecedented physical and chemical properties.[1–5] In recent years, some of abundantly produced EMFs have been well studied, and their potential applications in the fields of biomedicine,[6–8] material science,[9] and photovoltaics/photosynthesis[10–12] have been anticipated. On the other hand, to date, studies concerning the structural and electronic features of various less-known EMFs are still going on,[13–16] which aim to better understand the EMF family and therefore to advance this field.

Particularly, C$_{74}$ EMFs are less-known species. Despite several previously performed studies, only very few C$_{74}$-EMFs have been unambiguously characterized. This might be due to their low solubility or low availability. For instance, the La@C$_{74}$ with a trivalent metal is almost insoluble in most common organic solvents. This feature is similar to that of pristine C$_{74}$ and has been attributed to the ultra-small band gap of the pristine cage as suggested by the related theoretical calculations.[17] Upon exohedral chemical modification, the resulting derivative, that is, La@C$_{74}$(C$_6$H$_3$Cl$_2$),[18] has a much wider band

gap and therefore much better solubility relative to La@C$_{74}$. Thus, the structural and electrochemical characterizations of La@C$_{74}$(C$_6$H$_3$Cl$_2$) were well performed. On the other hand, the C$_{74}$ species that contain a divalent metal, namely M^{II}@C$_{74}$ (where M = Ca,[19] Ba,[20] Sr,[21] Eu,[22] Sm[23,24] or Yb[25,26]), are more soluble than empty C$_{74}$ and La@C$_{74}$. Specifically, Ba@C$_{74}$ and Ca@C$_{74}$, which contain a Group II metal, have been studied by means of single-crystal X-ray diffraction or NMR spectroscopy. They were revealed to have the same cage of D_{3h}-C$_{74}$ and both endohedral Group II metals exhibited jumps between the three symmetry-equivalent pyracylene units of the cage, reflecting a featured metal–cage interaction. However, M@C$_{74}$ that contains a divalent rare-earth metal has been never characterized for clarity. Considering the different electronic features of Group II metal ions and rare-earth metal ions, we therefore guess that encapsulating a rare-earth metal instead of a Group II metal may render some difference to the endohedral structure of EMF.

In the early studies, we have detected the presence of a moderate amount of Sm@C$_{74}$ (ref. 23 and 24) and Yb@C$_{74}$ (ref. 25 and 26) in the soot produced by direct current arc discharge of M–Ni alloy/C composite rods under a He atmosphere. However, because of the lack of further characterization, these species are still little known. Herein, we investigate the title compound by employing a combined study of single-crystal X-ray diffraction, DFT calculations and electrochemistry. The following discussions will focus on its structural features as well as the metal–cage interaction and the size of band gap.

Experimental

Synthesis and isolation

The synthesis of Sm-metallofullerenes was described in earlier studies.[27]

[a]Jiangsu Key Laboratory of Thin Films and School of Energy, Soochow University, Suzhou 215006, P. R. China. E-mail: fenglai@suda.edu.cn

[b]Beijing National Laboratory for Molecular Sciences, State Key Lab of Rare Earth Materials Chemistry and Applications, College of Chemistry and Molecular Engineering, Peking University, Beijing 100871, P. R. China. E-mail: zjshi@pku.edu.cn

[c]Department of Theoretical and Computational Molecular Science, Institute for Molecular Science, Okazaki 444-8585, Japan

[d]Department of Physical and Macromolecular Chemistry, Faculty of Science, Charles University in Prague, Albertov 6, 128 43 Praha 2, Czech Republic

† Electronic supplementary information (ESI) available. See DOI: 10.1039/c3nr03447j

Single-crystal X-ray diffraction analysis

Black co-crystals of Sm@D_{3h}-C$_{74}$/Ni^{II}(OEP) were obtained by allowing a benzene solution of fullerene and a chloroform solution of Ni^{II}(OEP) to diffuse together. X-ray data were collected at 90 K using a diffractometer (APEX II; Bruker Analytik GmbH) equipped with a CCD collector. The multi-scan method was used for absorption correction. The structure was resolved using direct methods (SHELXS97) and refined on F^2 using full-matrix least squares using SHELXL97.[28] The intact cage was modeled *via* the crystallographic mirror plane in refinement. Hydrogen atoms were added geometrically and refined with a riding model.

Electrochemistry

Differential pulse voltammetry (DPV) and cyclic voltammetry (CV) were carried out in *o*-dichlorobenzene (*o*-DCB) using a BAS CW-50 instrument. A conventional three-electrode cell consisting of a platinum working electrode, a platinum counter-electrode, and a saturated calomel reference electrode (SCE) was used for both measurements. 0.05 M (*n*-Bu)$_4$NPF$_6$ was used as the supporting electrolyte. All potentials were recorded against a SCE reference electrode and corrected against Fc/Fc$^+$. DPV and CV were measured at a scan rate of 20 and 100 mV s^{-1}, respectively.

Computational method

All calculations were carried out using the Gaussian 09 program package.[29] Geometry optimizations and Mulliken population analysis were performed using the density functional theory with the recently introduced M06-2X functional,[30] 3-21G basis set[31] for the C atom, and the SDD basis set[32] (with the SDD effective core potential) for Ni and Sm atoms (the M06-2X/3-21G~SDD level). The orbital energies were also calculated at a higher level (the M06-2X/6-31G~SDD level).

Results and discussion

The purity and the composition of the Sm@C$_{74}$ sample were confirmed by HPLC and MALDI-TOF mass, respectively (see Fig. S1†). The absorption spectrum of Sm@C$_{74}$ is almost identical to that reported previously,[23] as well as those of analogous species M@C$_{74}$ (M = Eu, Sr, Ba and Ca)[19–26] (See Fig. S2†). The absolute structure of Sm@D_{3h}-C$_{74}$ was identified *via* a single-crystal X-ray diffraction (XRD) study. Co-crystals of Sm@D_{3h}-C$_{74}$/[Ni^{II}(OEP)] suitable for X-ray analysis were obtained by slow diffusion of a benzene solution of EMF into a chloroform solution of [Ni^{II}(OEP)]. The molecular structure was resolved and refined in a monoclinic space group C_2 (no. 5).[33] Fig. 1 shows the X-ray structure of Sm@D_{3h}-C$_{74}$ together with an adjacent [Ni^{II}(OEP)] moiety. Note that the D_{3h}-C$_{74}$ cage has been crystallographically identified in two orientations with fractional occupancies of 0.67 and 0.33. Only the major cage is depicted in Fig. 1. The porphyrin moiety is approaching a flat region of the D_{3h}-C$_{74}$ cage with the shortest nickel-to-cage carbon distance ranging from 2.606 to 2.867 Å, indicating their strong π–π stacking interaction.
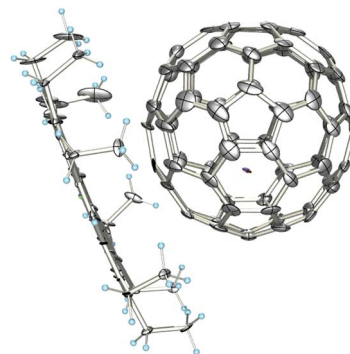

Fig. 1 Ortep drawing of Sm@D_{3h}-C$_{74}$·Ni^{II}(OEP) with 25% thermal ellipsoids, showing the intermolecular interaction. The major Sm site with fractional occupancy of 0.311 and the major cage position with fractional occupancy of 0.673 are depicted. The solvent molecules are omitted for clarity.

Inside the cage of D_{3h}-C$_{74}$, the Sm atom is highly disordered and several metal-sites have been refined with fractional occupancies ranging from 0.311 to 0.024, reflecting a motional behavior of the endohedral Sm atom. This feature is unlike that of previously reported Ba@C$_{74}$, in which only two different Ba positions were identified, corresponding well to the disordered cage, which is aligned in two orientations. Summarizing all the crystallographically characterized Sm-fullerenes that have different cage sizes and structures, it is noteworthy that such a dynamic endohedral feature is common for Sm-fullerenes,[34,35] indicating their weaker metal–cage interactions relative to those of other mono-metal-lofullerenes.[3,36] Considering the occupancies of cage and metal, we initially assigned the major Sm-site (*i.e.*, Sm01) to the major cage, as shown in Fig. 1, while another Sm-site with the second highest occupancy (*i.e.*, Sm02) was assigned to the minor cage, as shown in Fig. S3.† Such assignments give rise to a pair of identical conformers of Sm@C$_{74}$, in which the metal is localized off-center, being close to one of the three symmetry-equivalent pyracylene units at the horizontal mirror plane with a distance of 2.417 Å between the Sm and the central 6 : 6 bond of that pyracylene motif. Such a metal–cage alignment is very similar to that of Ba@C$_{74}$, confirming the previous assumption that there is a significant interaction between the pyracylene motif and the endohedral divalent metal. Nevertheless, this Sm-pyracylene motif interaction might be weaker than that in Ba@C$_{74}$, as reflected by the fact that the Sm atom can jump to other sites where the pyracylene unit is far from.

In addition, a series of computational studies were performed at the levels of M06-2x/3-21G~SDD and M06-2X/6-31G*~SDD to investigate the electronic features of Sm@C$_{74}$. As shown in Fig. 2, the DFT-optimized pristine Sm@D_{3h}-C$_{74}$ is in good agreement with the X-ray structure of Sm@D_{3h}-C$_{74}$. Particularly, the optimized Sm site is approaching the central 6 : 6 bond of a pyracylene unit with a distance of 2.533 Å, very close to that detected in the X-ray structure. Note that there are three equivalent pyracylene units on the cage of D_{3h}-C$_{74}$. However, if considering the influence of the adjacent
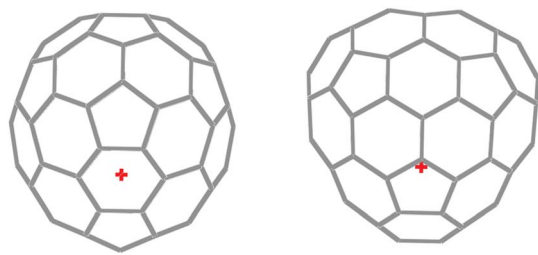
Fig. 2 Two views of DFT-optimized pristine Sm@D_{3h}-C_{74} at M06-2X/6-31G*~SDD level.

Fig. 4 HOMO (left) and LUMO (right) distributions of Sm@D_{3h}-C_{74} DFT-calculated at M06-2X/6-31G*~SDD level.

Ni^{II}(OEP) moiety, these pyracylene units are chemically non-equivalent. Therefore, we further optimize the unit of Sm@D_{3h}-C_{74}/[Ni^{II}(OEP)] to investigate the most preferred Sm-site relative to the adjacent Ni^{II}(OEP) moiety. Two DFT-optimized configurations of Sm@D_{3h}-C_{74}/[Ni^{II}(OEP)] are shown in Fig. 3 and S4† in different views. Particularly, in each configuration, the Sm site is close to one of the pyracylene units but differently aligned relative to the adjacent Ni^{II}(OEP) moiety. Calculations further revealed that the configuration shown in the left panel, which is fully consistent with the X-ray structure of Sm@D_{3h}-C_{74}/[Ni^{II}(OEP)] (see Fig. 1), is 0.079 kcal mol^{-1} more stable than that in the right panel. Although such a difference between the relative energies of these two configurations is very small, it is detectable at the present DFT level, suggesting a weak but salient influence of the porphyrin moiety on the location of endohedral metal.

HOMO and LUMO distributions of Sm@D_{3h}-C_{74} were calculated at a M06-2X/3-21G~SDD level, as shown in Fig. 4. Specifically, the HOMO is uniformly delocalized on the D_{3h}-C_{74} framework, while the LUMO is mostly localized on the cage area where the Sm is close to. The calculated Mulliken charge on the endohedral Sm atom is 2.04, indicative of a formal two-electron transfer from the metal to the cage. Thus, an ionic model of Sm^{2+}@(D_{3h}-C_{74})$^{2-}$ has been verified, which well describes the electronic feature of Sm@D_{3h}-C_{74}. Also, because of the off-center position of the endohedral divalent metal, the metal-donated charges are mainly
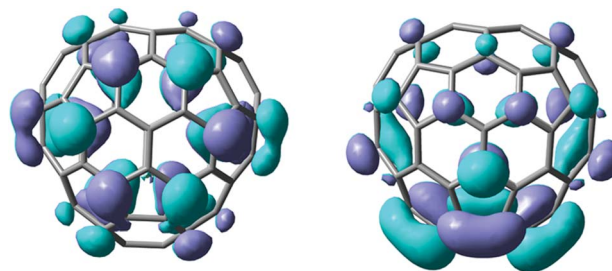
delocalized on the pyracylene motif and the nearby area, as suggested by the Mulliken population analysis. In particular, the carbons on the central 6 : 6 bond of that pyracylene motif are much more negatively charged than others (see Fig. S3 and Table S1†), indicating their higher nucleophilic affinity.

Furthermore, a comparison study between D_{3h}-C_{74}, (D_{3h}-C_{74})$^{2-}$ and Sm@D_{3h}-C_{74} was performed to estimate the role of the endohedral Sm atom in stabilizing the otherwise unstable D_{3h}-C_{74} cage. The DFT-calculated HOMO/LUMO energy levels of D_{3h}-C_{74}, (D_{3h}-C_{74})$^{2-}$ and Sm@D_{3h}-C_{74} are summarized in Fig. 5. The ultra-small band gap of D_{3h}-C_{74} (i.e., 1.65 eV) and the high HOMO/LUMO energy levels of (D_{3h}-C_{74})$^{2-}$ shall account for their low stabilities. In contrast, Sm@D_{3h}-C_{74} shows a band gap (i.e., 2.76 eV) larger than that of D_{3h}-C_{74} but smaller than that of (D_{3h}-C_{74})$^{2-}$. Besides, the lower-lying HOMO/LUMO of Sm@D_{3h}-C_{74} as compared with those of (D_{3h}-C_{74})$^{2-}$ is in line with its higher stability relative to the other. Thus, our computational studies show that the encapsulation of a divalent rare-earth metal can definitely improve the stability of a D_{3h}-C_{74} cage by rationalizing the size of band gap as well as the HOMO/LUMO energy levels.

The electrochemical properties of Sm@D_{3h}-C_{74} were investigated by means of cyclic voltammetry (CV) and differential pulse voltammetry (DPV). As shown in Fig. 6, both CV and DPV profiles suggest four reversible one-electron reductive steps on
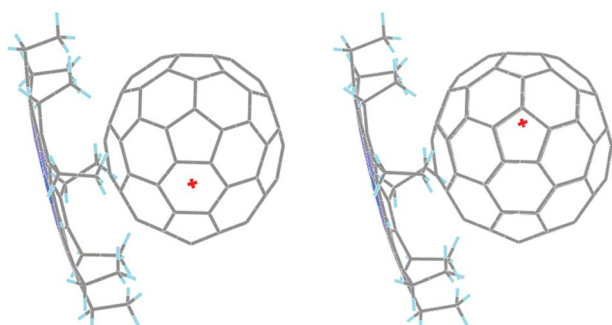

Fig. 3 Two DFT-optimized units of Sm@D_{3h}-C_{74}/[Ni^{II}(OEP)] at M06-2X/3-21G~SDD level.

Fig. 5 MO diagram for D_{3h}-C_{74}, (D_{3h}-C_{74})$^{2-}$ and Sm@D_{3h}-C_{74}. At M06-2X/3-21G~SDD level (their HOMO–LUMO gaps at M06-2X/6-31G*~SDD level are 1.72, 3.01 and 2.74 eV, respectively).

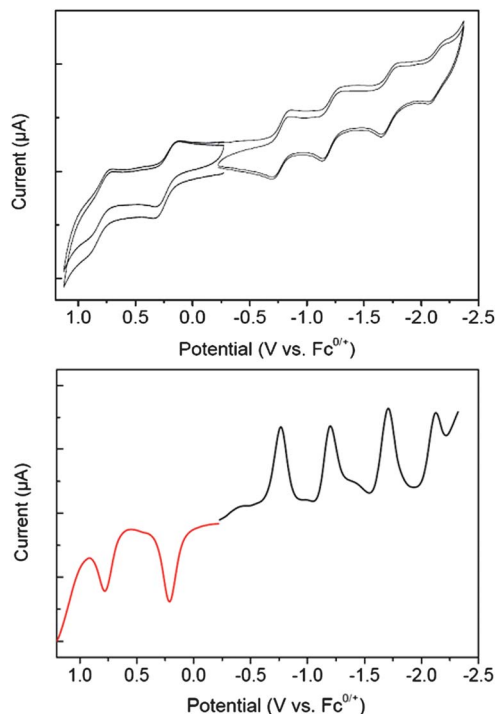**Fig. 6** Cyclic voltammograms (top) and differential pulse voltammogram (bottom) of Sm@D_{3h}-C$_{74}$ in o-DCB (0.05 M (n-Bu)$_4$NPF$_6$; scan rate: 100 mV s^{-1} and 20 mV s^{-1} for CV and DPV, respectively).

the cathodic side and two reversible one-electron oxidative steps on the anodic side. All the redox potentials obtained from CV are summarized in Table 1 and compared with those of other Sm-fullerenes such as Sm@C_{2v}(3)-C$_{80}$[34] and Sm@C_2(5)-C$_{82}$.[35] It is noteworthy that the first oxidation potential of Sm@D_{3h}-C$_{74}$ is 220–230 mV lower than those of middle-sized Sm-fullerenes, indicating a much stronger electron-donating ability. On the other hand, only a minor difference is found among the first reduction potentials of these Sm-fullerenes. Thus, the electrochemical potential gap of Sm@D_{3h}-C$_{74}$ is 0.97 eV, substantially smaller than those of other Sm-fullerenes (i.e., 1.28 eV for Sm@C_{2v}(3)-C$_{80}$ and 1.26 eV for Sm@C_2(5)-C$_{82}$), indicative of a smaller band gap relative to the others. This has been reflected by the fact that Sm@D_{3h}-C$_{74}$ shows lower solubility in common organic solvents. As a result, the resolution of the ^{13}C NMR spectrum of Sm@D_{3h}-C$_{74}$ was too low to be acceptable even after long-time scans because of the insufficient solubility of Sm@D_{3h}-C$_{74}$ in CS$_2$.

Table 1 Redox potentials (V vs. Fc$^{0/+}$)^a of Sm@D_{3h}-C$_{74}$ and other Sm-fullerenes

	$^{ox}E_2$	$^{ox}E_1$	$^{red}E_1$	$^{red}E_2$	$^{red}E_3$	$^{red}E_4$
Sm@D_{3h}-C$_{74}$	0.76^b	0.20^b	−0.77^b	−1.21^b	−1.72^b	−2.14^b
Sm@C_{2v}(3)-C$_{80}$^{d}	0.85^c	0.43^b	−0.85^b	−1.23^b	−1.76^b	−2.07^c
Sm@C_2(5)-C$_{82}$^{e}		0.42^c	−0.84^b	−1.01^b	−1.51^b	−1.90^b

^{a} Half-cell potentials unless otherwise noted. ^{b} Reversible process. ^{c} DPV value. ^{d} ref. 34. ^{e} ref. 35.

Conclusions

In conclusion, we have studied a divalent metallofullerene Sm@D_{3h}-C$_{74}$ structurally and electrochemically. Specifically, single-crystal X-ray diffraction analysis revealed that the endohedral Sm atom mainly binds to one pyracylene motif on the cage, which has been confirmed by computational studies. Nevertheless, the Sm–cage interaction is weaker than that in Ba@C$_{74}$, as reflected by the fact that the Sm atom more or less jumps to an other site far from the pyracylene motif. Thus, this study has confirmed that the variety of endohedral metal indeed imposes a salient influence on the metal–cage interaction and therefore affects the endohedral behavior. In addition, electrochemical studies demonstrated a smaller electrochemical potential gap of Sm@D_{3h}-C$_{74}$ relative to those of other Sm-fullerenes, indicative of a small band gap species.

Acknowledgements

Notes and references

1 T. Akasaka and S. Nagase, *Endofullerenes: A New Family of Carbon Clusters*, Kluwer, Dordrecht, The Netherlands, 2002.

2 M. N. Chaur, F. Melin, A. L. Ortiz and L. Echegoyen, *Angew. Chem., Int. Ed.*, 2009, **48**, 7514–7538.

3 X. Lu, L. Feng, T. Akasaka and S. Nagase, *Chem. Soc. Rev.*, 2012, **41**, 7723–7760.

4 J. Zhang, S. Stevenson and H. C. Dorn, *Acc. Chem. Res.*, 2013, **46**, 1548–1557.

5 A. A. Popov, S. Yang and L. Dunsch, *Chem. Rev.*, 2013, **113**, 5989–6113.

6 R. D. Bolskar, *Nanomedicine*, 2008, **3**, 201–213.

7 X. J. Liang, H. Meng, Y. Wang, H. He, J. Meng, J. Lu, P. C. Wang, Y. Zhao, X. Gao, B. Sun, C. Chen, G. Xing, D. Shen, M. M. Gottesman, Y. Wu, J. J. Yin and L. Jia, *Proc. Natl. Acad. Sci. U. S. A.*, 2010, **107**, 7449–7454.

8 J. D. Wilson, W. C. Broaddus, H. C. Dorn, P. P. Fatouros, C. E. Chalfant and M. D. Shultz, *Bioconjugate Chem.*, 2012, **23**, 1873–1880.

9 R. B. Ross, C. M. Cardona, D. M. Guldi, S. G. Sankaranarayanan, M. O. Reese, N. Kopidakis, J. Peet, B. Walker, G. C. Bazan, E. Van Keuren, B. C. Holloway and M. Drees, *Nat. Mater.*, 2009, **8**, 208–212.

10 L. Feng, Z. Slanina, S. Sato, K. Yoza, T. Tsuchiya, N. Mizorogi, T. Akasaka, S. Nagase, N. Martin and D. M. Guldi, *Angew. Chem., Int. Ed.*, 2011, **50**, 5909–5912.

11 M. Rudolf, S. Wolfrum, D. M. Guldi, L. Feng, T. Tsuchiya, T. Akasaka and L. Echegoyen, *Chem.–Eur. J.*, 2012, **18**, 5136–5148.

12 L. Feng, M. Rudolf, S. Wolfrum, A. Troeger, Z. Slanina, T. Akasaka, S. Nagase, N. Martin, T. Ameri, C. J. Brabec and D. M. Guldi, *J. Am. Chem. Soc.*, 2012, **134**, 12190–12197.

13 T.-S. Wang, N. Chen, J.-F. Xiang, B. Li, J.-Y. Wu, W. Xu, L. Jiang, K. Tan, C.-Y. Shu, X. Lu and C.-R. Wang, *J. Am. Chem. Soc.*, 2009, **131**, 16646–16647.

14 N. Chen, M. N. Chaur, C. Moore, J. R. Pinzon, R. Valencia, A. Rodriguez-Fortea, J. M. Poblet and L. Echegoyen, *Chem. Commun.*, 2010, **46**, 4818–4820.

15 W. Xu, L. Feng, M. Calvaresi, J. Liu, Y. Liu, B. Niu, Z. Shi, Y. Lian and F. Zerbetto, *J. Am. Chem. Soc.*, 2013, **135**, 4187–4190.

16 S. Yang, C. Chen, F. Liu, Y. Xie, F. Li, M. Jiao, M. Suzuki, T. Wei, S. Wang, Z. Chen, X. Lu and T. Akasaka, *Sci. Rep.*, 2013, **3**, 1487.

17 M. D. Diener and J. M. Alford, *Nature*, 1998, **393**, 668–671.

18 H. Nikawa, T. Kikuchi, T. Wakahara, T. Nakahodo, T. Tsuchiya, G. M. A. Rahman, T. Akasaka, Y. Maeda, K. Yoza, E. Horn, K. Yamamoto, N. Mizorogi and S. Nagase, *J. Am. Chem. Soc.*, 2005, **127**, 9684–9685.

19 T. Kodama, R. Fujii, Y. Miyake, S. Suzuki, H. Nishikawa, I. Ikemoto, K. Kikuchi and Y. Achiba, *Chem. Phys. Lett.*, 2004, **399**, 94–97.

20 A. Reich, M. Panthöfer, H. Modrow, U. Wedig and M. Jansen, *J. Am. Chem. Soc.*, 2004, **126**, 14428–14434.

21 O. Haufe, M. Hecht, A. Grupp, M. Mehring and M. Jansen, *Z. Anorg. Allg. Chem.*, 2005, **631**, 126–130.

22 P. Kuran, M. Krause, A. Bartl and L. Dunsch, *Chem. Phys. Lett.*, 1998, **292**, 580–586.

23 T. Okazaki, Y. Lian, Z. Gu, K. Suenaga and S. Hisanori, *Chem. Phys. Lett.*, 2000, **320**, 435–440.

24 T. Okazaki, K. Suenaga, Y. F. Lian, Z. N. Gu and H. Shinohara, *J. Mol. Graphics Modell.*, 2001, **19**, 244–251.

25 J. Xu, T. Tsuchiya, C. Hao, Z. Shi, T. Wakahara, W. Mi, Z. Gu and T. Akasaka, *Chem. Phys. Lett.*, 2006, **419**, 44–47.

26 J. Xu, X. Lu, X. Zhou, X. He, Z. Shi and Z. Gu, *Chem. Mater.*, 2004, **16**, 2959–2964.

27 J. Liu, Z. Shi and Z. Gu, *Chem.–Asian J.*, 2009, **4**, 1703–1711.

28 G. Sheldrick, *Acta Crystallogr., Sect. A: Found. Crystallogr.*, 2008, **64**, 112–122.

29 M. J. Frisch, G. W. Trucks, H. B. Schlegel, G. E. Scuseria, M. A. Robb, J. R. Cheeseman, G. Scalmani, V. Barone, B. Mennucci, G. A. Petersson, H. Nakatsuji, M. Caricato, X. Li, H. P. Hratchian, A. F. Izmaylov, J. Bloino, G. Zheng, J. L. Sonnenberg, M. Hada, M. Ehara, K. Toyota, R. Fukuda, J. Hasegawa, M. Ishida, T. Nakajima, Y. Honda, O. Kitao, H. Nakai, T. Vreven, J. A. Montgomery, Jr., J. E. Peralta, F. Ogliaro, M. Bearpark, J. J. Heyd, E. Brothers, K. N. Kudin, V. N. Staroverov, R. Kobayashi, J. Normand, K. Raghavachari, A. Rendell, J. C. Burant, S. S. Iyengar, J. Tomasi, M. Cossi, N. Rega, J. M. Millam, M. Klene, J. E. Knox, J. B. Cross, V. Bakken, C. Adamo, J. Jaramillo, R. Gomperts, R. E. Stratmann, O. Yazyev, A. J. Austin, R. Cammi, C. Pomelli, J. W. Ochterski, R. L. Martin, K. Morokuma, V. G. Zakrzewski, G. A. Voth, P. Salvador, J. J. Dannenberg, S. Dapprich, A. D. Daniels, O. Farkas, J. B. Foresman, J. V. Ortiz, J. Cioslowski and D. J. Fox, *Gaussian 09, Revision A.02*, Gaussian, Inc., Wallingford, CT, 2009.

30 Y. Zhao and D. Truhlar, *Theor. Chem. Acc.*, 2008, **120**, 215–241.

31 A. D. Becke, *J. Chem. Phys.*, 1993, **98**, 5648–5652.

32 X. Cao and M. Dolg, *THEOCHEM*, 2002, **581**, 139–147.

33 Crystal data for $Sm@D_{3h}$-C_{74}·Ni^{II}(OEP)·$0.75C_6H_6$·$0.25CHCl_3$: $C_{114.75}H_{48.75}Cl_{0.75}SmN_4Ni$, M_r = 1718.98, 0.16 × 0.14 × 0.05 mm, monoclinic, C_2, a = 25.082(6), b = 14.877(3), c = 19.229(4), β = 93.881(3)°, V = 7159(3) Å^3, Z = 4, ρ_{calc} = 1.595 g cm^{-3}, μ(MoKa) = 1.168 mm^{-1}, θ = 4.33–29.13°, T = 90 K, R_1 = 0.1326, wR_2 = 0.3365 for all data; R_1 = 0.1258, wR_2 = 0.3312 for 17431 reflections ($I > 2.0\sigma(I)$) with 1306 parameters. Maximum residual electron density 1.490 e Å^{-3}. CCDC 947376 presents supplementary crystallographic data for this paper.

34 W. Xu, B. Niu, Z. Shi, Y. Lian and L. Feng, *Nanoscale*, 2012, **4**, 6876–6879.

35 W. Xu, B. Niu, L. Feng, Z. Shi and Y. Lian, *Chem.–Eur. J.*, 2012, **18**, 14246–14249.

36 It appears that for most mono-metallofullerenes the mono-metal is highly localized, indicating a strong interaction between metal and a specific cage motif (see ref. 3). However, for di-metallofullerenes, the figure of cage indeed affects the endohedral behavior. For instance, in a round cage of C_{80} or C_{82}, dimetallic cluster rotates freely, as reflected by their high disorder (*i.e.*, $Er_2@C_{82}$ and $Ce_2@C_{80}$; see ref. 37–39). In these cases, not only metal–cage interaction but also metal–metal interaction shall be considered.

37 M. M. Olmstead, A. de Bettencourt-Dias, S. Stevenson, H. C. Dorn and A. L. Balch, *J. Am. Chem. Soc.*, 2002, **124**, 4172–4173.

38 M. M. Olmstead, H. M. Lee, S. Stevenson, H. C. Dorn and A. L. Balch, *Chem. Commun.*, 2002, 2688–2689.

39 L. Feng, M. Suzuki, N. Mizorogi, X. Lu, M. Yamada, T. Akasaka and S. Nagase, *Chem.–Eur. J.*, 2013, **19**, 988–993.